





Learning an SAR Image Despeckling Model Via Weighted Sparse Representation

Junchao Zhang , *Member, IEEE*, Jianlai Chen , *Member, IEEE*, Hanwen Yu , *Senior Member, IEEE*, Degui Yang, Xiaoqing Xu, and Mengdao Xing , *Fellow, IEEE*

Abstract—Synthetic aperture radar (SAR) images are inherently degraded by the speckle noise due to the coherent imaging, which may affect the performance of subsequent image analysis task. To address this problem, a weighted sparse representation-based method is proposed in this article for SAR image despeckling. The homomorphic transformation is first adopted to convert multiplicative noise into additive one. Second, similar patches are grouped together to learn the adaptive dictionaries and sparse coefficients based on nonlocal self-similarity constraint. Moreover, weighted regularizations are adopted for coefficients to boost the performance. Finally, despeckling images are obtained via exponential transformation. Experimental results on synthetic and real-world SAR images demonstrate that our proposed method outperforms several state-of-the-art methods in terms of both quantitative measurements and visual quality.

Index Terms—Despeckling, dictionary learning, nonlocal self-similarity, sparse representation, synthetic aperture radar (SAR).

I. INTRODUCTION

SYNTHETIC aperture radar (SAR) imaging has been widely used in the field of remote sensing owing to its all-day and all-weather acquisition capability. However, SAR images are inherently degraded by the speckle noise due to the coherent nature of the scattering phenomena. The speckle noise may hamper the performance of subsequent image analysis tasks such as terrain classification and target detection [1], [2]. Thus, SAR image despeckling is essential to improve the quality of the image, and it is usually a preprocessing operator for subsequent tasks.

In the past few decades, lots of despeckling methods have been proposed to recover noise-free SAR images from the degraded ones. The earlier proposed spatial-domain filters were Lee filter [3], Frost filter [4], and Kuan filter [5]. In these

methods, the SAR speckle noise is treated as a multiplicative one. Based on the local image statistics, despeckling is carried out according to the minimum-mean-square-error (MMSE) criterion or the maximum-a-posteriori (MAP) criterion. The despeckling performance is highly dependent on the parameters of the local window. Moreover, despeckling methods in the wavelet domain are also proposed. The homomorphic filtering is first adopted to convert multiplicative noise into additive one, then the speckle noise is removed based on the normal inverse Gaussian model [6]. The undecimated wavelet transform and the MAP criterion are combined, and the distribution of speckle noise in wavelet domain is approximated as a Laplacian and a Gaussian function [7]. Except for wavelet domain, similar image patches are denoised by the linear minimum mean-square error (LMMSE) filtering in principal component analysis (PCA) domain [8], [9]. These transform-domain-based methods are superior to the spatial-domain filters in terms of edge preservation, but they tend to generate artifacts [10].

In addition, nonlocal mean (NLM)-based denoising strategy is adopted in the field of SAR image despeckling, and the representative methods are the probabilistic patch-based (PPB) algorithm [11] and synthetic aperture radar block matching 3D (SARBM3D) [12]. This NLM-based approach utilizes the similarity between the targeted and its surrounding patches to obtain the weight for pixel averaging in a nonlocal region. In [13], the NLM-based methods are summarized with three steps: defining patch similarities, estimation of radar properties, and reprojection to image space. For the PPB [11], the statistical similarity criterion is proposed to select the most similar patches for a target patch, leading to better despeckling results than using the Euclidean distance measurement. Ferraioli *et al.* [14] propose a ratio-patch-based similarity criterion to select similar pixels. The ratio patch is defined between the patch containing the pixel to be restored and that containing a candidate similar pixel. Inspired by block matching 3D (BM3D, designed for Gaussian-distributed noise removing) [15], Parrilli *et al.* [12] propose the SARBM3D, aiming to remove the speckle noise in SAR images. In SARBM3D [12], the local linear MMSE estimation criterion and undecimated wavelet are adopted to boost the despeckling performance. Although SARBM3D [12] provides an excellent performance for SAR image despeckling, it is time consuming and unsuited to time-critical applications. A fast adaptive non-local SAR despeckling (FANS) [16] is proposed to reduce the execution time. The strategy of variable-size searching area and probabilistic early termination is adopted to speed up the block

Manuscript received January 28, 2021; revised May 16, 2021; accepted July 10, 2021. Date of publication July 14, 2021; date of current version July 28, 2021. This work was supported in part by the National Natural Science Foundation of China under Grant 61901531 and in part by the Foundation of Key Laboratory of National Defense Science and Technology under Grant 6142401200301. (Corresponding author: Jianlai Chen.)

Junchao Zhang, Jianlai Chen, Degui Yang, and Xiaoqing Xu are with the School of Aeronautics and Astronautics, Central South University, Changsha 410083, China (e-mail: junchaozhang@csu.edu.cn; jianlaichen@163.com; degui.yang@csu.edu.cn; xq_hsu@163.com).

Hanwen Yu is with the School of Resources and Environment, University of Electronic Science and Technology of China, Chengdu 611731, China (e-mail: yuhanwenxd@gmail.com).

Mengdao Xing is with the National Laboratory of Radar Signal Processing, Xidian University, Xi'an 710071, China (e-mail: xmd@xidian.edu.cn).

Digital Object Identifier 10.1109/JSTARS.2021.3097119

matching. Besides, the distance is calculated through lookup tables to accelerate this algorithm. The variational model-based methods provide another available way to remove the speckle noise, such as in [17] and [18], in which despeckling problems are transformed to minimize some energy functions.

In recent years, machine learning-based methods are proposed and show promising results in the field of SAR image despeckling [19]–[25]. These methods mainly include: low-rank representation [19], [20], sparse representation [21], [22], and deep convolutional neural network (CNN) [23]–[25]. In [19], similar patches are grouped and low-rank constraint is used to remove the speckle noise. Moreover, a boosting recursive method is adopted to boost the performance. For sparse representation-based model *patch ordering and transform domain filtering* (POTDF) [22], image patches are ordered and processed by two-stage filtering. The overcomplete dictionary is learned by the K singular value decomposition (KSVD) method [26] in the first stage, and then, 2-D wavelet is used for refined filtering. The overcomplete dictionary is not optimal to encode the whole image, and despeckling results are oversmooth (see experimental results). Since deep learning has been successfully adopted in the field of image restoration, Chierchia *et al.* [23] first propose the SAR-CNN for SAR image despeckling. This network is designed to recover additional noise by using logarithmic operation to input images. The network comprises 17 full convolutional layers, and the residual learning is used. Instead of using homomorphic transformation, an end-to-end despeckling network *image despeckling CNN* [24] is proposed. This network is trained using Euclidean measurement and total variation constraint as loss function. Moreover, the guided filtering is integrated into the CNN [25] to remove the speckle noise. All these deep learning-based methods do outperform the conventional methods on simulated data. However, these networks are learned in a supervised way and it is difficult to simulate all the noise conditions, yielding nonideal despeckling results for unknown noise in real applications.

In this article, a weighted sparse representation-based method is proposed for SAR image despeckling. As same as the most despeckling methods [19], [22], [23], the homomorphic transformation is first adopted to convert multiplicative noise into additive one. The similar patches are grouped together to learn the adaptive dictionaries. The nonlocal self-similarity constraint is adopted in the stage of dictionary learning. Moreover, for a target patch, weighted regularizations are adopted for coefficients to learn its sparse coefficients. Finally, despeckling images are obtained via exponential transformation and patch averaging. Experimental results on synthetic and real-world SAR images demonstrate that our proposed method outperforms several state-of-the-art methods in terms of quantitative measurements and visual quality. Our main contributions can be summarized as follows:

- 1) a weighted sparse representation model is proposed to address SAR image despeckling, which is different with the conventional model;
- 2) the local and compact dictionaries are learned instead of learning overcompleted ones, which is more suitable to encode different image structures.

II. SAR IMAGE DESPECKLING BASED ON WEIGHTED SPARSE REPRESENTATION

SAR image despeckling aims to recover a noise-free image \mathbf{x} from the degraded data \mathbf{y} , and the speckle noise \mathbf{n} is usually treated as multiplicative one [27]. The relationship between \mathbf{y} and \mathbf{x} can be formulated as

$$\mathbf{y} = \mathbf{x} \odot \mathbf{n} \quad (1)$$

where \odot denotes Hadamard product. As established in [27], the intensity of the speckle noise obeys the Gamma distribution. Thus, the probability density function of each element in noise can be defined as

$$p(n) = \frac{L^L n^{L-1}}{\Gamma(L)} \exp(-nL), \quad n \geq 0 \quad (2)$$

where L and $\Gamma(\cdot)$ are the equivalent number of looks (ENL) and the Gamma function, respectively. The ENL parameter can be estimated by the method in [28], which is a lookup-table-based one, so it is known for this task. To convert multiplicative noise into additive one, the logarithmic transformation is carried out to (1), and the model is rewritten as

$$\ln(\mathbf{y}) = \ln(\mathbf{x}) + \ln(\mathbf{n}). \quad (3)$$

Since the mean of $\ln(\mathbf{n})$ is nonzero, a bias correction [22] is used to (3). The corrected image \mathbf{y}_c can be formulated as

$$\mathbf{y}_c = \ln(\mathbf{y}) - \psi^{(0)}(L) + \ln(L) = \mathbf{x}_c + \mathbf{n}_c \quad (4)$$

where $\psi^{(r)}(\cdot)$ is the polygamma function with the order of r . \mathbf{x}_c and \mathbf{n}_c are the bias-corrected versions of $\ln(\mathbf{x})$ and $\ln(\mathbf{n})$, respectively. The distribution of bias-corrected noise tends to become Gaussian with the increase of ENL [22], thus \mathbf{n}_c can be treated as Gaussian-distributed noise to be removed. According to the sparse representation theory [29], [30], the SAR image despeckling question can be transformed to minimize the following problem:

$$\{\Phi^*, \alpha^*\} = \arg \min_{\Phi, \alpha} \left\{ \|\mathbf{y}_c - \Phi \alpha\|_2^2 + \lambda \|\alpha\|_1 \right\} \quad (5)$$

where λ is regularization parameter, and Φ and α represent dictionary and sparse coefficients, respectively. After obtaining dictionary Φ^* and sparse coefficients α^* , the noise-free image can be recovered as $\mathbf{x} = \exp(\Phi^* \alpha^*)$.

Instead of directly learning the dictionary and sparse coefficients [formulated in (5)] on the whole image, the commonly used strategy of patch processing is adopted. For a $p \times p$ patch, it is extracted from $\mathbf{x}_c \in \mathbb{R}^{MN}$ and denoted by $\mathbf{x}_i = R_i(\mathbf{x}_c) \in \mathbb{R}^{p^2}$, where $R_i(\cdot)$ is the extracting operator and $R_i(\mathbf{x}_c)$ denotes that the i th patch is extracted from \mathbf{x}_c ; and M and N represent the number of row and column, respectively. Correspondingly, the i th patch of \mathbf{y}_c can be denoted by \mathbf{y}_i . Equation (5) is modified as follows:

$$\min_{\Phi_i, \alpha_i} \left\{ \|\mathbf{y}_i - \Phi_i \alpha_i\|_2^2 + \lambda_i \|\alpha_i\|_1 \right\}, \quad i = 1, 2, 3, \dots, K \quad (6)$$

where K is the number of extracted patches, and $K = (\lceil M - p \rceil / s + 1) * (\lceil N - p \rceil / s + 1)$ with the stride of s . Thus, SAR image despeckling problem is transformed to learn dictionary and sparse coefficients for each patch.

TABLE I
PSNR RESULTS ON THE TEN TESTING IMAGES UNDER SIMULATED SPECKLE NOISE

Image		Monarch	Barbara	Boat	Cameraman	Couple	Hill	House	Man	Peppers	Straw	Average
$L = 1$	Noisy	12.62	12.28	11.74	12.03	12.37	12.82	11.33	12.87	12.00	10.12	12.018
	POTDF	15.57	15.27	14.74	14.91	15.40	15.92	14.37	15.94	15.39	12.76	15.027
	PPB	22.51	24.11	24.24	23.01	23.63	25.03	25.53	24.83	24.20	18.70	23.579
	SARBM3D	24.36	25.38	25.44	24.95	25.31	26.45	27.59	26.01	25.62	19.98	25.109
	FANS	24.40	24.75	25.27	25.33	24.91	26.08	27.11	25.76	25.64	19.01	24.826
	Ours_nw	22.68	23.93	23.98	23.90	23.64	24.80	25.46	24.52	24.10	18.88	23.589
	Ours	24.02	24.63	24.45	24.91	24.10	25.21	26.46	24.97	24.88	18.97	24.260
$L = 4$	Noisy	18.24	17.99	17.45	17.69	18.06	18.54	17.01	18.55	17.66	15.79	17.698
	POTDF	22.28	22.10	23.14	23.59	23.36	24.16	23.06	23.91	24.02	18.20	22.782
	PPB	25.66	27.47	26.98	26.26	27.02	28.06	29.47	27.58	27.16	22.20	26.786
	SARBM3D	27.87	29.16	28.38	27.95	28.60	29.35	31.13	28.83	28.65	23.42	28.334
	FANS	28.17	29.24	28.31	28.36	28.64	29.22	31.07	28.67	28.97	23.37	28.402
	Ours_nw	26.16	26.73	25.91	25.94	26.28	26.97	26.86	26.71	26.38	22.55	26.049
	Ours	28.66	29.69	28.40	28.56	28.65	29.19	31.60	28.66	29.09	23.86	28.636
$L = 16$	Noisy	24.32	23.94	23.40	23.71	24.01	24.50	23.00	24.52	23.70	21.83	23.693
	POTDF	26.89	25.92	26.65	28.30	26.38	26.88	28.50	26.83	28.02	20.30	26.467
	PPB	28.93	30.17	29.90	28.86	29.93	30.84	32.27	30.34	30.15	25.11	29.650
	SARBM3D	31.42	32.08	31.38	31.46	31.73	32.18	34.19	31.81	32.10	26.70	31.505
	FANS	31.90	32.58	31.54	31.81	31.90	32.31	34.14	31.92	32.47	27.08	31.765
	Ours_nw	27.93	27.85	27.22	27.48	27.74	28.33	27.31	28.19	27.55	24.84	27.444
	Ours	32.66	33.29	31.68	32.03	32.02	32.34	34.59	32.07	32.71	27.75	32.114

Best results are in bold font.



Fig. 1. Ten testing images. From left to right and top to bottom: Monarch, Barbara, Boat, Cameraman, Couple, Hill, House, Man, Peppers, and Straw.

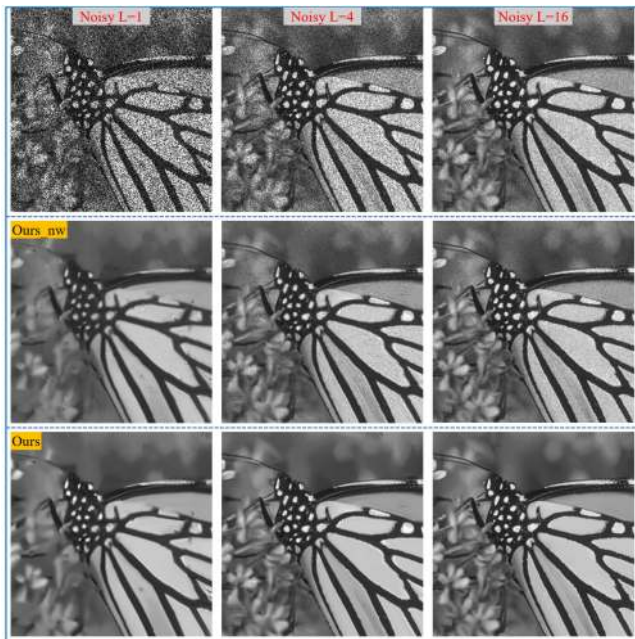


Fig. 2. Despeckling results under different noise levels on the *Monarch* testing image. From the second row to bottom, despeckling results are obtained by using *Ours_nw* and *ours*.

A. Dictionary Learning

The local and compact dictionary learning [29]–[31] is commonly used in the field of image restoration and it shows promising results. To better encode the local structure of SAR images, a local and compact dictionary learning is adopted instead of learning a globally overcomplete dictionary.

For a patch \mathbf{x}_i , its nonlocal self-similar patches can be obtained in a large enough window according to the distance with \mathbf{x}_i . The statistical similarity criterion is proposed to select the most similar patches for a target patch, leading to better despeckling results than using the Euclidean distance measurement [11]. Thus, the distance between \mathbf{x}_i and \mathbf{x}_j can be formulated as

$$d(\mathbf{x}_i, \mathbf{x}_j) = \sum_{k=1}^{p^2} \ln \left[\sqrt{\frac{x_i(k)}{x_j(k)}} + \sqrt{\frac{x_j(k)}{x_i(k)}} \right]. \quad (7)$$

A patch \mathbf{x}_{ik} is selected as a similar patch to \mathbf{x}_i if the distance d is not greater than a preset threshold. In fact, the first m most similar patches are selected, and they are grouped together, denoted by $\mathbf{X}_i = [\mathbf{x}_{i1}, \mathbf{x}_{i2}, \dots, \mathbf{x}_{im}] \in \mathbb{R}^{p^2 \times m}$. Thus, the adaptive dictionary Φ_i of \mathbf{x}_i can be obtained using singular value decomposition as

$$\mathbf{X}_i = \mathbf{V}\mathbf{\Lambda}\mathbf{V}^T = \Phi_i\mathbf{\Lambda}\mathbf{V}^T \quad (8)$$

where Φ_i is an orthonormal matrix composed by the eigenvectors, and $\mathbf{\Lambda}$ is the diagonal matrix of eigenvalues. Since the eigenvectors represent the structural variations and are used to encode the image patches [32], the dictionary is learned based on (8).

B. Sparse Coefficients Updating

Based on the learned dictionary, the sparse coefficients of \mathbf{x}_i can be obtained according to (6). However, the larger the eigenvalue is, the more important the corresponding eigenvector in Φ_i is. Thus, the sparse coefficient over the eigenvector should

TABLE II
 SSIM RESULTS ON THE TEN TESTING IMAGES UNDER SIMULATED SPECKLE NOISE

Image		Monarch	Barbara	Boat	Camerman	Couple	Hill	House	Man	Peppers	Straw	Average
$L = 1$	Noisy	0.25	0.20	0.15	0.28	0.17	0.14	0.10	0.15	0.17	0.20	0.181
	POTDF	0.51	0.52	0.51	0.58	0.49	0.52	0.59	0.54	0.60	0.16	0.502
	PPB	0.71	0.66	0.58	0.67	0.55	0.55	0.65	0.60	0.68	0.29	0.594
	SARBM3D	0.79	0.73	0.65	0.76	0.66	0.65	0.76	0.68	0.75	0.44	0.687
	FANS	0.80	0.71	0.65	0.79	0.63	0.63	0.77	0.67	0.77	0.27	0.669
	Ours_nw	0.74	0.68	0.60	0.73	0.58	0.57	0.71	0.62	0.72	0.29	0.624
	Ours	0.79	0.72	0.62	0.77	0.60	0.58	0.76	0.64	0.76	0.28	0.652
$L = 4$	Noisy	0.45	0.40	0.31	0.42	0.35	0.34	0.23	0.34	0.33	0.47	0.364
	POTDF	0.72	0.58	0.58	0.75	0.57	0.56	0.68	0.60	0.74	0.16	0.594
	PPB	0.83	0.81	0.70	0.78	0.72	0.71	0.78	0.74	0.79	0.66	0.752
	SARBM3D	0.89	0.86	0.76	0.84	0.79	0.77	0.83	0.79	0.84	0.75	0.812
	FANS	0.90	0.86	0.74	0.85	0.78	0.75	0.84	0.78	0.85	0.73	0.808
	Ours_nw	0.75	0.72	0.61	0.65	0.65	0.65	0.59	0.66	0.67	0.72	0.667
	Ours	0.90	0.87	0.75	0.84	0.79	0.75	0.84	0.78	0.85	0.77	0.814
$L = 16$	Noisy	0.65	0.63	0.53	0.57	0.58	0.60	0.44	0.59	0.55	0.75	0.589
	POTDF	0.85	0.73	0.67	0.82	0.67	0.63	0.79	0.69	0.82	0.36	0.703
	PPB	0.90	0.89	0.81	0.87	0.83	0.82	0.86	0.84	0.87	0.85	0.854
	SARBM3D	0.94	0.92	0.84	0.91	0.87	0.87	0.89	0.88	0.90	0.89	0.891
	FANS	0.95	0.92	0.84	0.91	0.87	0.86	0.87	0.87	0.90	0.89	0.888
	Ours_nw	0.77	0.75	0.66	0.67	0.71	0.72	0.60	0.72	0.69	0.84	0.713
	Ours	0.95	0.93	0.84	0.91	0.87	0.86	0.89	0.88	0.90	0.91	0.894

Best results are in bold font.

be less sparse. The weighted sparse representation model can be formulated as

$$\min_{\alpha_i} \left\{ \|\mathbf{y}_i - \Phi_i \alpha_i\|_2^2 + \|\mathbf{w}_i^T \alpha_i\|_1 \right\}, i = 1, 2, 3, \dots, K \quad (9)$$

where \mathbf{w}_i is the weighted vector and it is related to the eigenvalues. Moreover, \mathbf{w}_i can be determined in the perspective of MAP estimation

$$\alpha_i^* = \arg \max_{\alpha_i} \{ \ln(P(\mathbf{y}_i | \alpha_i)) + \ln(P(\alpha_i)) \}. \quad (10)$$

The first term $\ln(P(\mathbf{y}_i | \alpha_i))$ corresponds to the likelihood, and it can be characterized by the distribution of noise. Hence, we have

$$P(\mathbf{y}_i | \alpha_i) = \frac{1}{\sqrt{2\pi}\sigma_i} \exp\left(-\frac{\|\mathbf{y}_i - \Phi_i \alpha_i\|_2^2}{2\sigma_i^2}\right) \quad (11)$$

where $\sigma_i^2 = \psi^{(1)}(L)$ is the standard deviation of noise [33]. The prior term $P(\alpha_i)$ is assumed to follow the Laplacian distribution, and all elements are independent and identically distributed. Thus

$$P(\alpha_i) = \prod_{k=1}^{p^2} \left(\frac{c}{\sqrt{2}\lambda_k} \exp\left(-\frac{c\sqrt{2}|\alpha_i(k)|}{\lambda_k}\right) \right) \quad (12)$$

where $\lambda_k = \sqrt{\text{diag}(\Lambda_k)}$ and c is a constant. Substituting (11) and (12) into (10), we have

$$\min_{\alpha_i} \left\{ \|\mathbf{y}_i - \Phi_i \alpha_i\|_2^2 + \sum_{k=1}^{p^2} \frac{c * 2\sqrt{2}\sigma_i^2}{\lambda_k} |\alpha_i(k)| \right\}. \quad (13)$$

Compared with (9), the weighted vector \mathbf{w}_i is estimated as

$$\mathbf{w}_i(k) = (c * 2\sqrt{2}\sigma_i^2) \lambda_k. \quad (14)$$

Algorithm 1: Despeckling via weighted sparse representation.

Input: Noisy image \mathbf{y}

Bias correction: According to (4)

Initialization: iterator $t = 0$, maximum iteration number

$T = 8$ and set:

(1) $\mathbf{x}_i^{(0)} = \mathbf{y}_i, \mathbf{y}_i^{(0)} = \mathbf{y}_i$.

(2) parameters: $p = 6, s = 3, m = 60$ and $c = 1/\sqrt{2}$.

Main Iteration: Increase t by 1 and perform the following steps:

1. Learning dictionary $\{\Phi_i\}_{i=1}^K$ by (8).

2. Updating sparse coefficients $\{\alpha_i\}_{i=1}^K$ by (15).

3. Updating $\mathbf{x}_i^{(t+1)}$ by (16) and $\mathbf{y}_i^{(t+1)} = \mathbf{x}_i^{(t+1)}$.

4. Updating $\sigma_i^{(t+1)} = (\sigma_i^2 - \|\mathbf{y}_i - \mathbf{y}_i^{(t+1)}\|_2^2)^{1/2}$.

5. Stopping rule: if $t > T$, stop. Otherwise, do another iteration.

Output: Noise-free image \mathbf{x} .

Thus, the sparse coefficients of \mathbf{x}_i can be updated by using the iterative shrinkage method [34]

$$\alpha_i = \text{soft}(\Phi_i^T \mathbf{y}_i, \mathbf{w}_i/2) \quad (15)$$

where $\text{soft}(a, b) = \max(|a| - b, 0) \cdot \text{sgn}(a)$. After obtaining the dictionary and sparse coefficients, the noise-free image can be reconstructed by

$$\mathbf{x} = \exp\left(\left(\sum_{i=1}^K R_i^T R_i\right)^{-1} \left(\sum_{i=1}^K R_i^T \Phi_i \alpha_i\right)\right). \quad (16)$$

The despeckling algorithm is summarized in Algorithm 1. The number of selected similar patch m is set to 60 experimentally, and m is generally greater than $p^2 = 36$. The parameter c is set to $1/\sqrt{2}$ for simplifying calculation.

TABLE III
FOM RESULTS ON THE TEN TESTING IMAGES UNDER SIMULATED SPECKLE NOISE

Image		Monarch	Barbara	Boat	Camerman	Couple	Hill	House	Man	Peppers	Straw	Average
$L = 1$	Noisy	0.24	0.21	0.12	0.15	0.15	0.12	0.10	0.12	0.14	0.13	0.148
	POTDF	0.44	0.28	0.40	0.55	0.33	0.32	0.58	0.40	0.27	0.22	0.379
	PPB	0.90	0.66	0.62	0.92	0.50	0.49	0.68	0.57	0.79	0.31	0.644
	SARBM3D	0.90	0.83	0.73	0.91	0.73	0.69	0.82	0.72	0.84	0.64	0.781
	FANS	0.91	0.71	0.67	0.91	0.59	0.59	0.77	0.64	0.81	0.45	0.705
	Ours_nw	0.89	0.77	0.69	0.88	0.62	0.62	0.72	0.66	0.76	0.55	0.716
	Ours	0.91	0.81	0.66	0.90	0.57	0.54	0.71	0.61	0.78	0.54	0.703
$L = 4$	Noisy	0.61	0.39	0.20	0.38	0.27	0.20	0.16	0.20	0.33	0.30	0.304
	POTDF	0.82	0.30	0.43	0.82	0.39	0.34	0.51	0.37	0.63	0.23	0.484
	PPB	0.95	0.93	0.84	0.96	0.84	0.80	0.91	0.82	0.92	0.57	0.854
	SARBM3D	0.95	0.94	0.86	0.96	0.89	0.86	0.92	0.84	0.92	0.78	0.892
	FANS	0.96	0.93	0.85	0.96	0.88	0.84	0.92	0.83	0.91	0.74	0.882
	Ours_nw	0.96	0.93	0.89	0.96	0.89	0.85	0.90	0.87	0.91	0.83	0.899
	Ours	0.96	0.93	0.88	0.96	0.89	0.86	0.93	0.84	0.91	0.72	0.888
$L = 16$	Noisy	0.96	0.80	0.69	0.93	0.73	0.50	0.53	0.57	0.85	0.65	0.721
	POTDF	0.95	0.79	0.74	0.94	0.64	0.61	0.80	0.68	0.81	0.71	0.767
	PPB	0.98	0.96	0.95	0.98	0.91	0.89	0.93	0.91	0.96	0.86	0.933
	SARBM3D	0.98	0.97	0.95	0.98	0.95	0.94	0.96	0.92	0.96	0.90	0.951
	FANS	0.99	0.97	0.95	0.98	0.95	0.93	0.96	0.91	0.95	0.90	0.949
	Ours_nw	0.99	0.96	0.95	0.98	0.95	0.92	0.94	0.93	0.96	0.92	0.950
	Ours	0.99	0.97	0.96	0.98	0.96	0.94	0.96	0.93	0.96	0.87	0.952

Best results are in bold font.

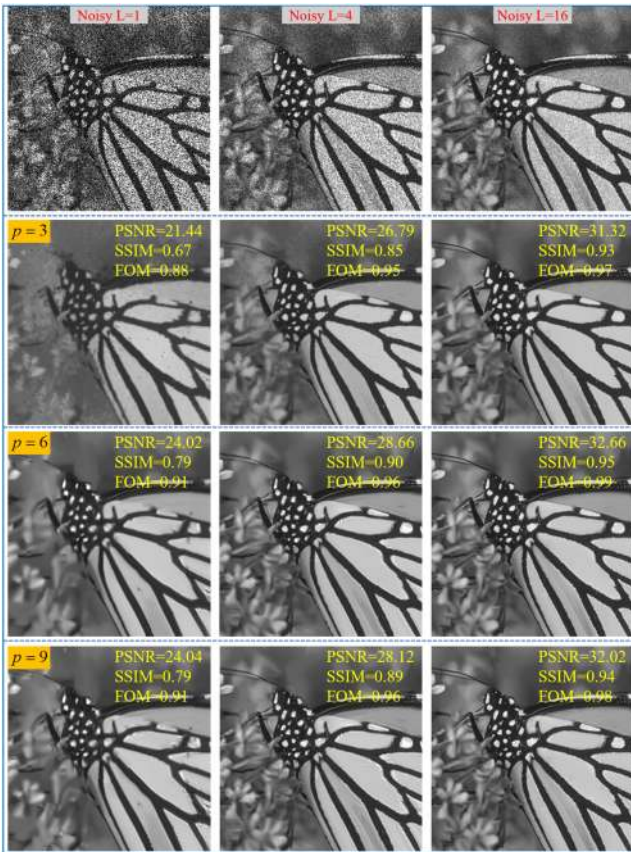


Fig. 3. Despeckling results under different noise levels on the *Monarch* testing image. From the second row to bottom, despeckling results are obtained by using the patch size $p = 3$, $p = 6$, and $p = 9$.

TABLE IV
RESULTS OF RUNNING TIME FOR DIFFERENT METHODS

	POTDF	PPB	SARBM3D	FANS	Ours
Running time (s)	4.63	9.94	14.65	1.41	36.37

III. EXPERIMENTAL RESULTS

In this section, both synthetic and real-world SAR images are used to test the performance of the proposed method. Moreover, an ablation experiment is carried out to verify the advantage of weighted sparse representation. For synthetic SAR images, ten testing images are used, as shown in Fig. 1. The synthetic SAR images are obtained by multiplying optical images by simulated white speckle in amplitude format, which is as same as that used in [12], and the ENL are set 1, 4, and 16. Real-world SAR data (*OurSAR*) are captured by sensors mounted on an airplane (3GHz, sliding spotlight mode, X band, resolution: 0.05 m \times 0.05 m), and images are obtained by using the autofocus method in [35]–[37]. Besides, the *AIRSAR* image (taken over Flevoland in Netherlands, used in [22]) and *TerraSAR* image (X band, HH polarization, resolution: 5 m \times 5 m, used in [18]) are also adopted to evaluate the performance.

The proposed method is compared with four state-of-the-art methods, such as POTDF [22], PPB [11], SARBM3D [12], and FANS [16]. The codes of all these methods are provided by the original authors. Since FANS [16] and SARBM3D [12] produce comparable results (see quantitative results), only the despeckling results of SARBM3D are displayed for visual comparison. Moreover, for simulated SAR images, the peak signal to noise ratio (PSNR), structural similarity (SSIM) [38], and Pratt’s figure of merit (FOM) [39] are used as the objective indexes to evaluate the performance. The β -ratio index [40] is also used to evaluate the despeckling performance for real data. The code of our proposed method can be downloaded from <https://github.com/Junchao2018/SAR-Image-Despeckling-WSC>.

A. Ablation Experiment

The ablation experiment is designed to verify that weighted regularization is beneficial to the despeckling performance. The despeckling results without weighted regularization are denoted by “Ours_nw,” i.e., the sparse coefficients are updated

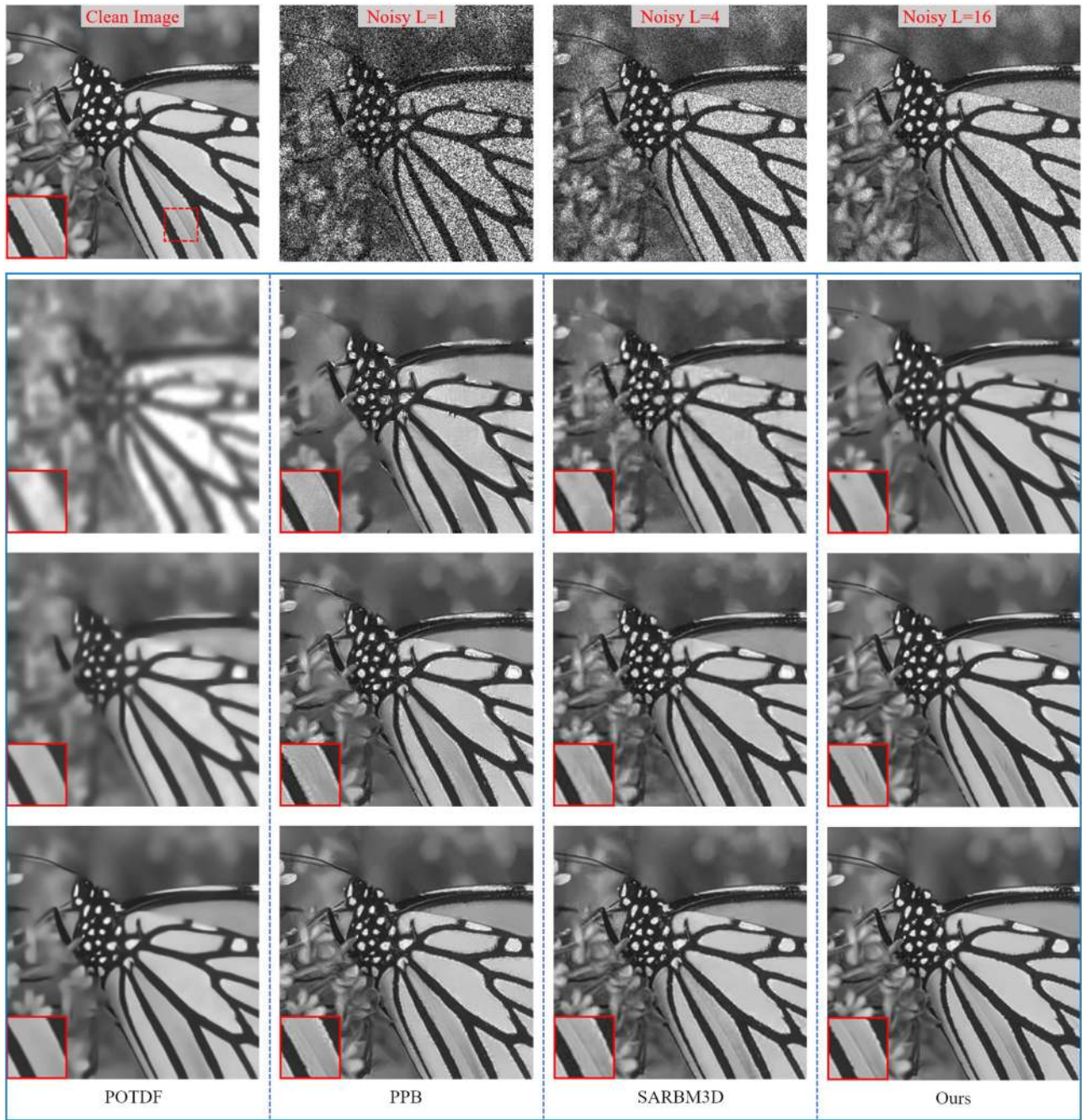


Fig. 4. Despeckling results of different methods under different noise levels on the *Monarch* testing image. From the second row to bottom and left to right, despeckling results are obtained by using POTDF, PPB, SARBM3D, and ours.

using (6). The experimental results are shown in Fig. 2, we can see that weighted regularization does boost the despeckling performance. The larger the eigenvalue is, the more important the corresponding eigenvector is. Thus, the sparse coefficient over the eigenvector should be less sparse. The weights are designed to control the sparsity of coefficients, producing better despeckling results. The quantitative comparisons are listed in Tables I–III. Based on the PSNR and SSIM values, one can see that the indexes are highly improved after adopting weighted regularization, and the FOM results are comparable.

The influence of a patch size on the despeckling performance is also analyzed. Three patch sizes ($p = 3$, $p = 6$, and $p = 9$) are used to evaluate the performance. The despeckling results on *Monarch* are shown in Fig. 3, and the noisy images are displayed in the first row. From the second row to bottom, despeckling results are obtained by using the patch size $p = 3$, $p = 6$, and $p = 9$, respectively. Meanwhile, the values of quantitative indexes (PSNR, SSIM, and FOM) are inserted at the top-right region of an image. One can see that the despeckling results are noisy at smaller patch size. A smaller patch size is corresponding to a smaller dictionary, which is not enough

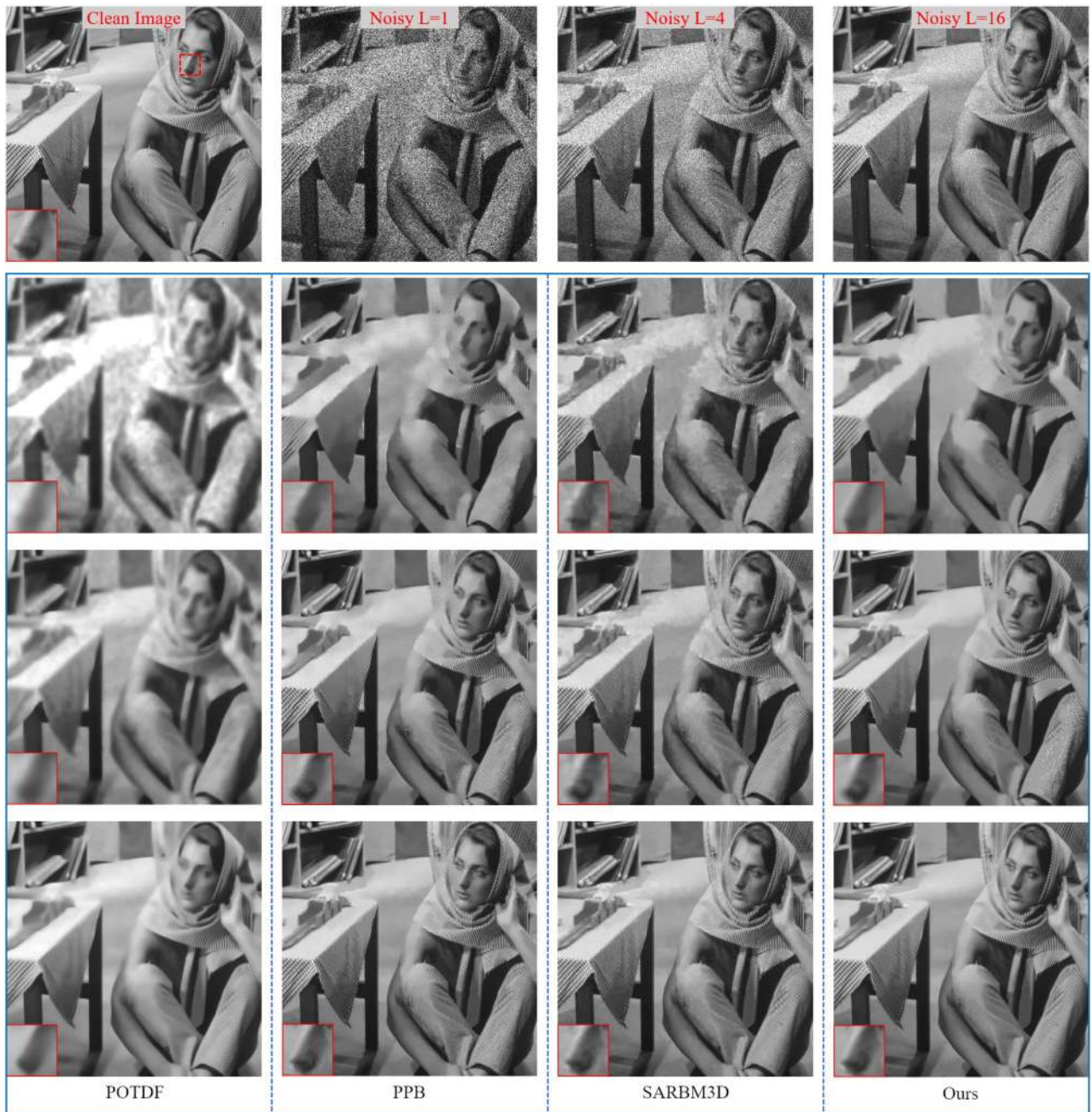


Fig. 5. Despeckling results of different methods under different noise levels on the *Barbara* testing image. From the second row to bottom and left to right, despeckling results are obtained by using POTDF, PPB, SARBM3D, and ours.

to encode different structures. The performances are comparable for $p = 6$ and $p = 9$, and larger patch size consume more computing resources. Thus, the patch size is set to 6 in our experiment.

B. Experimental Results on Simulated Data

Despeckling results of different methods on the *Monarch* testing image are shown in Fig. 4. The noisy images are generated with different values of ENL, and they are presented in the first row. The despeckling results of different methods are displayed from left to right. From the second row to the bottom, the results

are corresponding to $L = 1$, $L = 4$, and $L = 16$. The left-bottom regions are the enlarged views of the red dotted rectangles. The POTDF method [22] produces oversmooth results and the performance is bad for $L = 1$ case. A globally overcomplete dictionary is learned in the POTDF method [22], and it is not optimal to encode all structures, yielding oversmooth results. The NLM-based method PPB [11] produce better results than POTDF. However, it generates false artifacts at edges. The despeckling performance is improved by SARBM3D [12], which is because of adopting local linear MMSE estimation criterion and undecimated wavelet filtering. The despeckling results of ours are presented in the last column. One can see that the

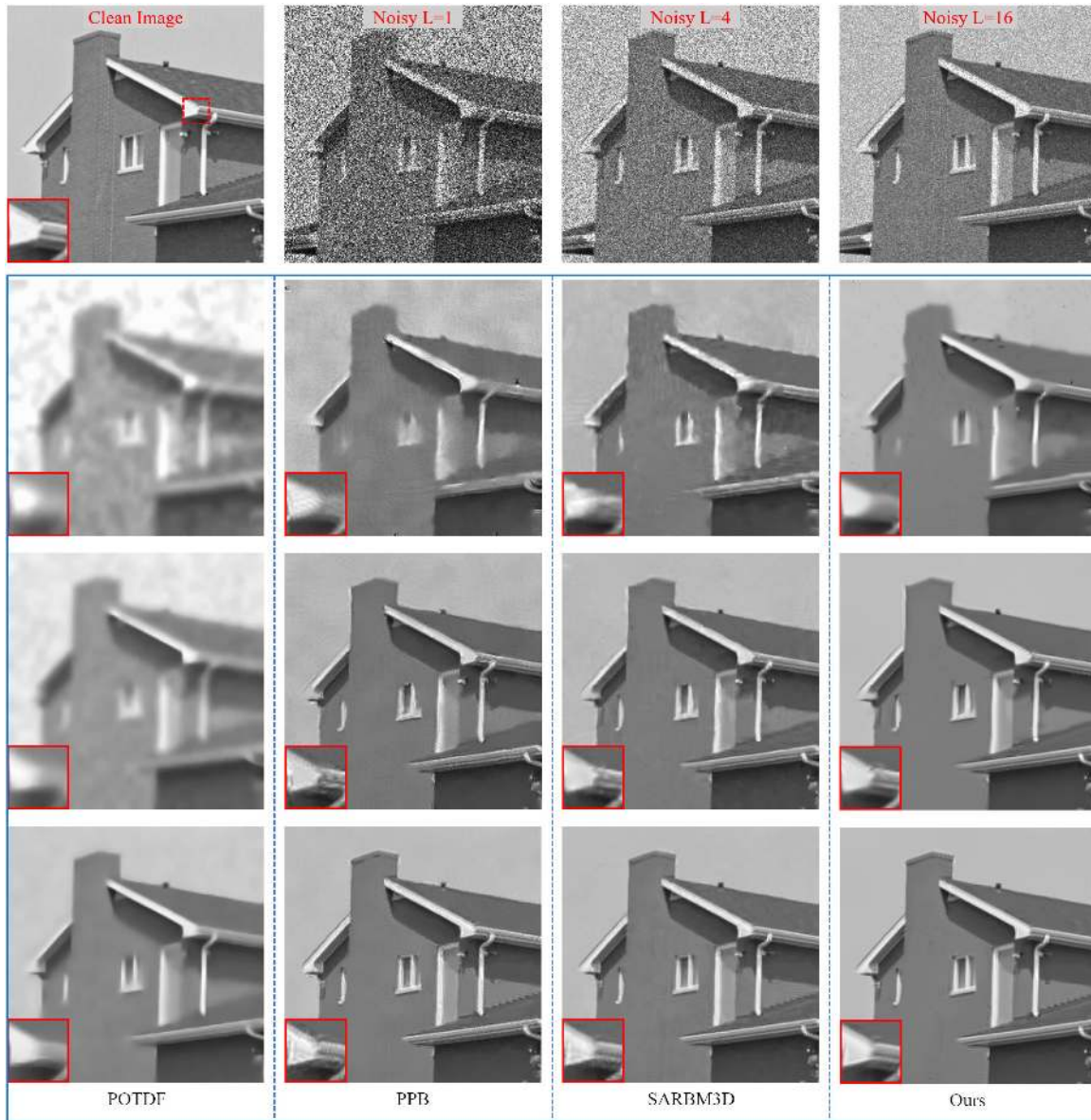


Fig. 6. Despeckling results of different methods under different noise levels on the *House* testing image. From the second row to bottom and left to right, despeckling results are obtained by using POTDF, PPB, SARBM3D, and ours.

recovered images of our method are clean while persevering image details (such as the enlarged regions) under larger ENL number. Although the result of our method is smoother than that of SARBM3D under heavy noise ($L = 1$), the most image details are recovered using our method. Moreover, the recovered images of SARBM3D are a little noisy at edges. Despeckling results on the *Barbara* and *House* testing images are shown in Figs. 5 and 6, respectively. The experimental results on these two testing images also demonstrate that our proposed method is superior to others.

Besides, the quantitative indexes are used to evaluate the despeckling performance, and the results are calculated on ten testing images. Table I presents the PSNR values of different methods under different ENL values, and the SSIM and FOM results are shown in Tables II and III, respectively. The larger the index is, the better the result is. The best result has been in

bold in the table. One can see that the PSNR and SSIM values of POTDF [22] are much smaller than that of other methods. The SARBM3D [12] achieves the highest PSNR and FOM values under $L = 1$, and our methods is the best at $L = 4$ and $L = 16$ in terms of PSNR and SSIM, which demonstrates that our method outperforms others at larger ENL number. For FOM index at larger ENL number, the SARBM3D [12], FANS [16], and our proposed method are comparable.

Moreover, the running time is evaluated on a machine with 3.6 GHz Intel Core i9-9900 K CPU (64 G RAM). For POTDF [22], PPB [11], SARBM3D [12], and FANS [16], the codes have been optimized by *Mex* compiling. Our code is implemented based on pure MATLAB language. For images with size of 256×256 , the averaged execution times are listed in Table IV. One can see that FANS is the fastest and accelerates the speed of SARBM3D by a large margin. Our method is more

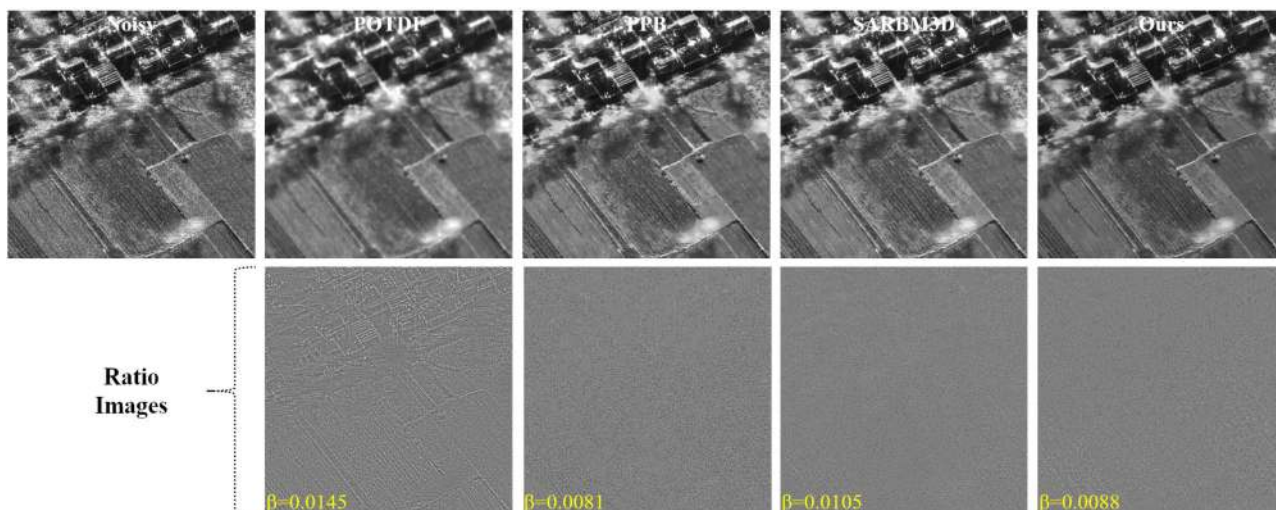


Fig. 7. Despeckling results (first row) and ratio images (second row) of different methods on *OurSAR* images. From left to right: Noisy images, despeckling results obtained by using POTDF, PPB, SARBM3D, and ours.

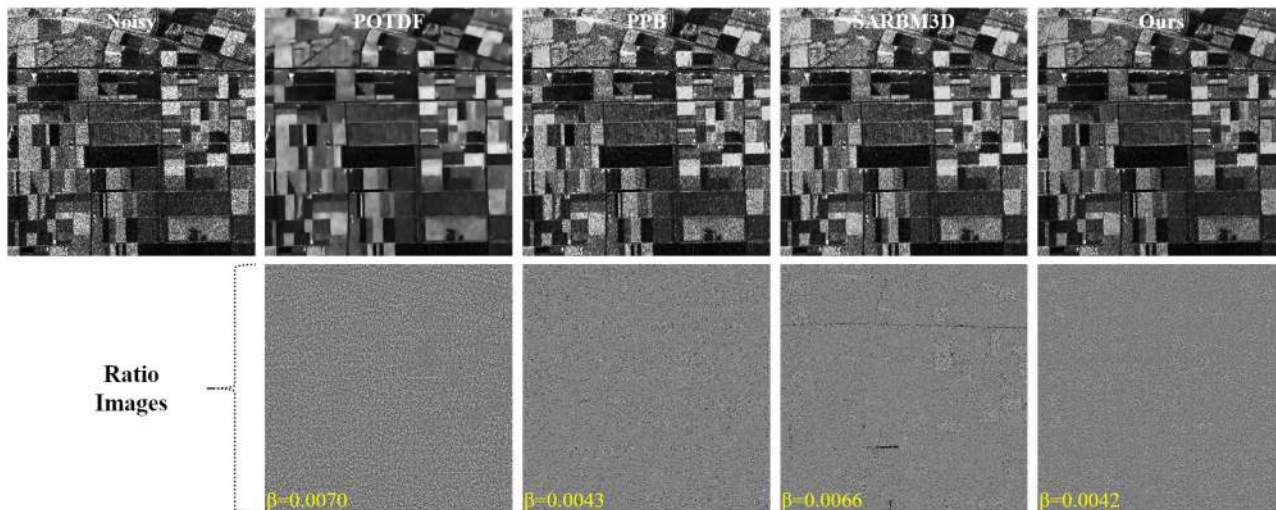


Fig. 8. Despeckling results (first row) and ratio images (second row) of different methods on *AIRSAR* images. From left to right: Noisy images, despeckling results obtained by using POTDF, PPB, SARBM3D, and ours.

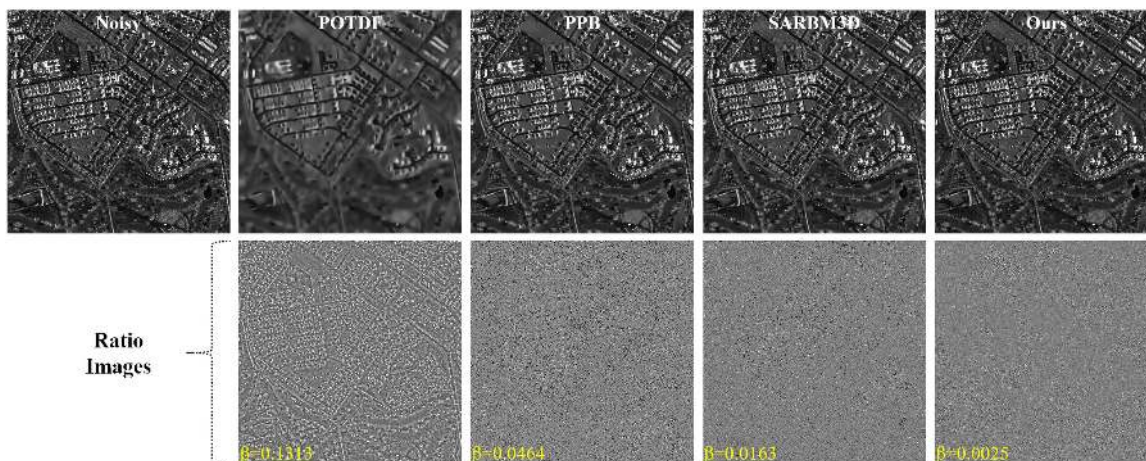


Fig. 9. Despeckling results (first row) and ratio images (second row) of different methods on *TerraSAR* images. From left to right: Noisy images, despeckling results obtained by using POTDF, PPB, SARBM3D, and ours.

time consuming than others without any code optimizing, while the codes of other methods are optimized. In the same way, code optimization, parallel computation, and GPU acceleration can be adopted to accelerate our method in the future.

C. Experimental Results on Real Data

Real-world SAR images are also used to test the performance. The despeckling results on three real scenes are shown in Figs. 7–9, respectively. The noisy images are presented in the first column, and despeckling results by POTDF [22], PPB [11], SARBM3D [12], and ours are displayed from the second column to right. The ratio images (defined as the ratio between the noisy image and the filtered one) are listed at the second row. Moreover, the β -ratio index is inserted at the left-bottom of ratio images. The smaller the β -ratio index is, the better the result is. For the *OurSAR* image shown in Fig. 7, the POTDF method [22] produces oversmooth results. The speckle noise is effectively removed by the PPB algorithm [11], but it generates distorted details at edges. The distorted edges are mitigated in the results produced by the SARBM3D approach [12] and ours. The ratio image acquired by a good filter should be a pure random noise process. On the contrary, the ratio image obtained by an inferior filter contains structural information, especially at urban areas and edges [22]. In the perspective of ratio images, our proposed method produces the best results. The despeckling results (as shown Figs. 8 and 9) on other two real-world SAR images also demonstrate that our method outperforms others.

IV. CONCLUSION

In this article, we propose a sparse representation-based model to remove speckle noise for SAR images. This model is learned in an unsupervised way, and it does not need abundant samples to be trained, which makes our method more practical. For multiplicative speckle noise, the homomorphic transformation is adopted to convert it into additive one. Based on nonlocal self-similarity constraint, similar patches are grouped together to learn the adaptively compact dictionaries and sparse coefficients, instead of learning globally overcomplete dictionaries. Moreover, weighted regularizations are adopted for coefficients to boost the performance. Finally, despeckling images are obtained via exponential transformation. Experimental results on synthetic and real-world SAR images demonstrate that our proposed method outperforms several state-of-the-art methods in terms of both quantitative measurements and visual quality.

Most deep learning-based despeckling networks are trained in a supervised way, and it is difficult to simulate all the noise conditions in the training stage. In the future, we will integrate the data-driven network into sparse representation model, investigating another available way for speckle noise removing.

REFERENCES

- [1] X. Ma, H. Shen, J. Yang, L. Zhang, and P. Li, "Polarimetric-spatial classification of SAR images based on the fusion of multiple classifiers," *IEEE J. Sel. Topics Appl. Earth Observ. Remote Sens.*, vol. 7, no. 3, pp. 961–971, Mar. 2014.
- [2] S. Huang, D. Liu, G. Gao, and X. Guo, "A novel method for speckle noise reduction and ship target detection in SAR images," *Pattern Recognit.*, vol. 42, no. 7, pp. 1533–1542, 2009.
- [3] J. Lee, "Digital image enhancement and noise filtering by use of local statistics," *IEEE Trans. Pattern Anal. Mach. Intell.*, vol. PAMI-2, no. 2, pp. 165–168, Mar. 1980.
- [4] V. S. Frost, J. A. Stiles, K. S. Shanmugan, and J. C. Holtzman, "A model for radar images and its application to adaptive digital filtering of multiplicative noise," *IEEE Trans. Pattern Anal. Mach. Intell.*, vol. PAMI-4, no. 2, pp. 157–166, Mar. 1982.
- [5] D. Kuan, A. Sawchuk, T. Strand, and P. Chavel, "Adaptive restoration of images with speckle," *IEEE Trans. Acoust., Speech, Signal Process.*, vol. 35, no. 3, pp. 373–383, Mar. 1987.
- [6] S. Solbo and T. Eltoft, "Homomorphic wavelet-based statistical despeckling of SAR images," *IEEE Trans. Geosci. Remote Sens.*, vol. 42, no. 4, pp. 711–721, Apr. 2004.
- [7] F. Argenti, T. Bianchi, A. Lapini, and L. Alparone, "Fast map despeckling based on Laplacian-Gaussian modeling of wavelet coefficients," *IEEE Geosci. Remote Sens. Lett.*, vol. 9, no. 1, pp. 13–17, Jan. 2012.
- [8] L. Xu, J. Li, Y. Shu, and J. Peng, "SAR image denoising via clustering-based principal component analysis," *IEEE Trans. Geosci. Remote Sens.*, vol. 52, no. 11, pp. 6858–6869, Nov. 2014.
- [9] B. Wang, C. Zhao, and Y. Liu, "An improved SAR interferogram denoising method based on principal component analysis and the Goldstein filter," *Remote Sens. Lett.*, vol. 9, no. 1, pp. 81–90, 2018.
- [10] K. Savithri and G. Kowsalya, "SAR image despeckling using Bandlet transform with firefly algorithm," *Int. J. Adv. Eng. Technol.*, vol. 7, no. 2, pp. 364–370, 2016.
- [11] C. Deledalle, L. Denis, and F. Tupin, "Iterative weighted maximum likelihood denoising with probabilistic patch-based weights," *IEEE Trans. Image Process.*, vol. 18, no. 12, pp. 2661–2672, Dec. 2009.
- [12] S. Parrilli, M. Poderico, C. V. Angelino, and L. Verdoliva, "A nonlocal SAR image denoising algorithm based on LLMMSE wavelet shrinkage," *IEEE Trans. Geosci. Remote Sens.*, vol. 50, no. 2, pp. 606–616, Feb. 2012.
- [13] C.-A. Deledalle, L. Denis, G. Poggi, F. Tupin, and L. Verdoliva, "Exploiting patch similarity for SAR image processing: The nonlocal paradigm," *IEEE Signal Process. Mag.*, vol. 31, no. 4, pp. 69–78, Jul. 2014.
- [14] G. Ferraioli, V. Pascazio, and G. Schirrinzi, "Ratio-based nonlocal anisotropic despeckling approach for SAR images," *IEEE Trans. Geosci. Remote Sens.*, vol. 57, no. 10, pp. 7785–7798, Oct. 2019.
- [15] K. Dabov, A. Foi, V. Katkovnik, and K. Egiazarian, "Image denoising by sparse 3D transform-domain collaborative filtering," *IEEE Trans. Image Process.*, vol. 16, no. 8, pp. 2080–2095, Aug. 2007.
- [16] D. Cozzolino, S. Parrilli, G. Scarpa, G. Poggi, and L. Verdoliva, "Fast adaptive nonlocal SAR despeckling," *IEEE Geosci. Remote Sens. Lett.*, vol. 11, no. 2, pp. 524–528, Feb. 2014.
- [17] G. Aubert and J.-F. Aujol, "A variational approach to removing multiplicative noise," *SIAM J. Appl. Math.*, vol. 68, no. 4, pp. 925–946, 2008.
- [18] M. Guo, C. Han, W. Wang, S. Zhong, and Z. Liu, "A novel truncated nonconvex nonsmooth variational method for SAR image despeckling," *Remote Sens. Lett.*, vol. 12, no. 2, pp. 174–183, 2020.
- [19] J. Fang, S. Hu, and X. Ma, "A boosting SAR image despeckling method based on non-local weighted group low-rank representation," *Sensors*, vol. 18, no. 10, 2018, Art. no. 3448.
- [20] G. Chen, G. Li, Y. Liu, X. Zhang, and L. Zhang, "SAR image despeckling based on combination of fractional-order total variation and nonlocal low rank regularization," *IEEE Trans. Geosci. Remote Sens.*, vol. 58, no. 3, pp. 2056–2070, Mar. 2020.
- [21] B. Xu, Y. Cui, Z. Li, and J. Yang, "An iterative SAR image filtering method using nonlocal sparse model," *IEEE Geosci. Remote Sens. Lett.*, vol. 12, no. 8, pp. 1635–1639, Aug. 2015.
- [22] B. Xu, Y. Cui, Z. Li, B. Zuo, J. Yang, and J. Song, "Patch ordering-based SAR image despeckling via transform-domain filtering," *IEEE J. Sel. Topics Appl. Earth Observ. Remote Sens.*, vol. 8, no. 4, pp. 1682–1695, Apr. 2015.
- [23] G. Chierchia, D. Cozzolino, G. Poggi, and L. Verdoliva, "SAR image despeckling through convolutional neural networks," in *Proc. IEEE Int. Geosci. Remote Sens. Symp.*, 2017, pp. 5438–5441.
- [24] P. Wang, H. Zhang, and V. M. Patel, "SAR image despeckling using a convolutional neural network," *IEEE Signal Process. Lett.*, vol. 24, no. 12, pp. 1763–1767, Dec. 2017.
- [25] S. Liu *et al.*, "Convolutional neural network and guided filtering for SAR image denoising," *Remote Sens.*, vol. 11, no. 6, 2019, Art. no. 702.
- [26] M. Aharon, M. Elad, and A. Bruckstein, "K-SVD: An algorithm for designing overcomplete dictionaries for sparse representation," *IEEE Trans. Signal Process.*, vol. 54, no. 11, pp. 4311–4322, Nov. 2006.
- [27] C. Oliver and S. Quegan, *Understanding Synthetic Aperture Radar Images* Boston USA: SciTech Publishing, 2004.

- [28] Y. Cui, G. Zhou, J. Yang, and Y. Yamaguchi, "Unsupervised estimation of the equivalent number of looks in SAR images," *IEEE Geosci. Remote Sens. Lett.*, vol. 8, no. 4, pp. 710–714, Jul. 2011.
- [29] W. Dong, X. Li, L. Zhang, and G. Shi, "Sparsity-based image denoising via dictionary learning and structural clustering," in *Proc. IEEE Conf. Comput. Vis. Pattern Recognit.*, 2011, pp. 457–464.
- [30] W. Dong, L. Zhang, G. Shi, and X. Li, "Nonlocally centralized sparse representation for image restoration," *IEEE Trans. Image Process.*, vol. 22, no. 4, pp. 1620–1630, Apr. 2013.
- [31] J. Zhang *et al.*, "Sparse representation-based demosaicing method for microgrid polarimeter imagery," *Opt. Lett.*, vol. 43, no. 14, pp. 3265–3268, 2018.
- [32] J. Xu, L. Zhang, W. Zuo, D. Zhang, and X. Feng, "Patch group based nonlocal self-similarity prior learning for image denoising," in *Proc. IEEE Int. Conf. Comput. Vis.*, 2015, pp. 244–252.
- [33] H. Xie, L. E. Pierce, and F. T. Ulaby, "Statistical properties of logarithmically transformed speckle," *IEEE Trans. Geosci. Remote Sens.*, vol. 40, no. 3, pp. 721–727, Mar. 2002.
- [34] I. Daubechies, M. Defriese, and C. DeMol, "An iterative thresholding algorithm for linear inverse problems with a sparsity constraint," *Commun. Pure Appl. Math.*, vol. 57, no. 11, pp. 1413–1457, 2004.
- [35] J. Chen, J. Zhang, Y. Jin, H. Yu, B. Liang, and D. Yang, "Real-time processing of spaceborne SAR data with nonlinear trajectory based on variable PRF," *IEEE Trans. Geosci. Remote Sens.*, early access, doi: [10.1109/TGRS.2021.3067945](https://doi.org/10.1109/TGRS.2021.3067945).
- [36] J. Chen, M. Xing, G. Sun, and Z. Li, "A 2D space-variant motion estimation and compensation method for ultrahigh-resolution airborne stepped-frequency SAR with long integration time," *IEEE Trans. Geosci. Remote Sens.*, vol. 55, no. 11, pp. 6390–6401, Nov. 2017.
- [37] J. Chen, B. Liang, D. Yang, D. Zhao, M. Xing, and G. Sun, "Two-step accuracy improvement of motion compensation for airborne SAR with ultrahigh resolution and wide swath," *IEEE Trans. Geosci. Remote Sens.*, vol. 57, no. 9, pp. 7148–7160, Sep. 2019.
- [38] Z. Wang, A. C. Bovik, H. R. Sheikh, and E. P. Simoncelli, "Image quality assessment: From error visibility to structural similarity," *IEEE Trans. Image Process.*, vol. 13, no. 4, pp. 600–612, Apr. 2004.
- [39] V. Bhadouria, "Pratt's figure of merit," Accessed: Mar. 2021. [Online]. Available: <https://www.mathworks.com/matlabcentral/fileexchange/60473-pratt-s-figure-of-merit>
- [40] L. Gomez, M. E. Buemi, J. C. Jacobo-Berlles, and M. E. Mejail, "A new image quality index for objectively evaluating despeckling filtering in SAR images," *IEEE J. Sel. Topics Appl. Earth Observ. Remote Sens.*, vol. 9, no. 3, pp. 1297–1307, Mar. 2016.



Junchao Zhang (Member, IEEE) received the B.S. degree in mechanical engineering and automation from HoHai University, Nanjing, China, in 2014, and the Ph.D. degree in pattern recognition and intelligent systems from the Shenyang Institute of Automation, Chinese Academy of Sciences, Beijing, China, in 2019.

From 2017 to 2018, he was a Visiting Joint Ph.D. Student with the University of Arizona. He has authored or coauthored more than 30 research articles in high-impact peer-reviewed journals. The total citation times of his research are greater than 240 (H-index 11). He is currently with the School of Aeronautics and Astronautics, Central South University, Changsha, China. His research interests include polarization imaging, synthetic aperture radar imaging, image processing, machine learning, and pattern recognition.



Jianlai Chen (Member, IEEE) was born in Hengyang, China, in 1990. He received the B.S. degree in electronic engineering and the Ph.D. degree in signal and information processing from Xidian University, Xi'an, China, in 2013 and 2018, respectively.

He is currently an Associate Professor with Central South University, Changsha, China. He has authored or coauthored one book and more than 20 research articles in high-impact peer-reviewed journals. His research interests include synthetic aperture radar (SAR) imaging, SAR motion compensation and autofocus, and machine learning.

Dr. Chen is the Guest Editor for the Special Issues of the *Remote Sensing and MDPI Sensors*.



Hanwen Yu (Senior Member, IEEE) received the B.S. and Ph.D. degrees in electronic engineering from the Xidian University, Xi'an, China, in 2007 and 2012, respectively.

He was a Postdoctoral Research Fellow with the Department of Civil and Environmental Engineering, National Center for Airborne Laser Mapping, University of Houston, Houston, TX, USA. He is currently a Full Professor with the School of Resources and Environment, University of Electronic Science and Technology of China, Chengdu, China. He has authored or coauthored more than 35 research articles in high-impact peer-reviewed journals including the *IEEE TRANSACTIONS ON GEOSCIENCE AND REMOTE SENSING*, *IEEE TRANSACTIONS ON IMAGE PROCESSING*, and *Remote Sensing of Environment*. His research interests include phase unwrapping, machine learning, and synthetic aperture radar interferometry signal processing and applications.

Prof. Yu has reviewed more than 200 manuscripts for more than 20 different journals. He was the recipient of the Recognition of Best Reviewer of the *IEEE TRANSACTIONS ON GEOSCIENCE AND REMOTE SENSING* in 2019. He serves as a Topical Associate Editor for the *IEEE TRANSACTIONS ON GEOSCIENCE AND REMOTE SENSING*, and an Associate Editor for the *IEEE GEOSCIENCE AND REMOTE SENSING MAGAZINE*. He has guest edited five special issues on InSAR remote sensing for different journals (e.g., *IEEE JOURNAL OF SELECTED TOPICS IN APPLIED EARTH OBSERVATIONS AND REMOTE SENSING* and *MDPI Sensors*).



Degui Yang received the B.S. degree in microwave and the M.S. and Ph.D. degrees in information and communication engineering from the National University of Defense Technology, Changsha, China, in 1999, 2002, and 2011 respectively.

He is currently a Full Professor with the School of Aeronautics and Astronautics, Central South University. He has authored or coauthored two books and more than 20 papers. His research interests include radar target characteristic, radar signal processing, and electronic warfare.



Xiaoqing Xu received the B.S. degree in 2020 in detection guidance and control technology from Central South University, Changsha, China, where she is currently working toward the master's degree in aeronautical and astronautical science and technology.

Her research interests include synthetic aperture radar imaging, image processing, and machine learning.



Mengdao Xing (Fellow, IEEE) received the B.S. and Ph.D. degrees from Xidian University, Xi'an, China, in 1997 and 2002, respectively.

He is currently a Professor with the National Laboratory of Radar Signal Processing, Xidian University, where He is also the Dean with the Academy of Advanced Interdisciplinary Research Department. He has authored and coauthored more than 200 refereed scientific journal papers and two books about synthetic aperture radar (SAR) signal processing. The total citation times of his research are greater than

10000 (H-index 50). He has achieved more than 50 authorized China patents. His current research interests include SAR, SAR interferometry, inversed synthetic aperture radar, sparse signal processing, and microwave remote sensing.

Dr. Xing was rated as Most-Cited Chinese Researchers by Elsevier. His research has been supported by various funding programs, including, National Science Fund for Distinguished Young Scholars. He has held several Special Issues on the *IEEE GEOSCIENCE AND REMOTE SENSING MAGAZINE* and *IEEE JOURNAL OF SELECTED TOPICS IN APPLIED EARTH OBSERVATIONS AND REMOTE SENSING*. He is currently the Associate Editors for radar remote sensing of the *IEEE TRANSACTIONS ON GEOSCIENCE AND REMOTE SENSING* and the Editor-in-Chief of *MDPI Sensors*.